Constraints on Nonrelativistic-QCD Long-Distance Matrix Elements from J/ψ Plus W/Z Production at the LHC

Mathias Butenschoen and Bernd A. Kniehl
II. Institut für Theoretische Physik, Universität Hamburg, Luruper Chaussee 149, 22761 Hamburg, Germany

(Received 22 July 2022; accepted 21 December 2022; published 23 January 2023)

We study the associated production of prompt J/ψ mesons and W or Z bosons within the factorization approach of nonrelativistic QCD (NRQCD) at next-to-leading order in α_s, via intermediate color singlet ${}^3S_1^{[1]}$ and ${}^3P_J^{[1]}$ and color octet ${}^1\mathrm{S}_0^{[8]}$, ${}^3\mathrm{S}_1^{[8]}$, and ${}^3\mathrm{P}_J^{[8]}$ states. Requiring for our predictions to be compatible with recent ATLAS measurements yields stringent new constraints on charmonium long-distance matrix elements (LDMEs) being nonperturbative, process-independent input parameters. Considering four popular LDME sets fitted to data of single J/ψ inclusive production, we find that one is marginally compatible with the data, with central predictions typically falling short by a factor of 3, one is unfavored, the factor of shortfall being about 1 order of magnitude, and two violate cross section positivity for direct $J/\psi + W/Z$ production. The large rate of prompt J/ψ plus W production observed by ATLAS provides strong evidence for the color octet mechanism inherent to NRQCD factorization, the leading color singlet contribution entering only at $\mathcal{O}(G_F\alpha_s^4)$, beyond the order considered here.

DOI: 10.1103/PhysRevLett.130.041901

Although heavy quarkonia have been discovered already in 1974, the underlying mechanisms governing their production in high-energy collisions are still not fully understood. The most prominent approach is via the factorization theorem of nonrelativistic QCD (NRQCD) [1,2]. According to it, the production cross section of quarkonium H factorizes into perturbative short-distance cross sections of heavy quark-antiquark bound-state production and supposedly universal nonperturbative long-distance matrix elements (LDMEs) $\langle\mathcal{O}^H(n)\rangle$, where $n = {}^{2S+1}L_J^{[1,8]}$ denotes the quarkonic Fock state, in color singlet "[1]" or octet "[8]" configuration. Velocity (v) scaling rules [3] impose a strong hierarchy on the $\langle\mathcal{O}^H(n)\rangle$ values, leading to a double expansion in the strong-coupling constant α_s and v. For $H = J/\psi$ and $\psi(2S)$, the LDMEs of $n = {}^3\mathrm{S}_1^{[1]}$ are leading in v and those of $n = {}^1\mathrm{S}_0^{[8]}$, ${}^3\mathrm{S}_1^{[8]}$, and ${}^3\mathrm{P}_J^{[8]}$ are subleading. For $H = \chi_{cJ}$, the LDMEs of $n = {}^3\mathrm{P}_J^{[1]}$ and ${}^3S_1^{[8]}$ are both leading in v.

The available charmonium LDME sets have all been extracted from data of single inclusive production. Thanks to the high luminosity meanwhile achieved by the LHC, also double production and associated production with bottomonia, W, and Z bosons have been studied there, which can inject orthogonal information into LDME determinations. The goal of this Letter is to provide the first complete analysis of prompt-J/ψ plus W or Z hadroproduction at next-to-leading order (NLO) in α_s, i.e., through $\mathcal{O}(G_F\alpha_s^3)$. Invoking QCD and NRQCD factorization, we calculate the cross sections as

$$\sigma(pp \to J/\psi + W/Z + X) = \sum_H \mathrm{Br}(H \to J/\psi) \sum_n \tilde{\sigma}(pp \to c\bar{c}[n] + W/Z + X)\langle\mathcal{O}^H(n)\rangle, \tag{1}$$

$$\tilde{\sigma}(pp \to c\bar{c}[n] + W/Z + X) = \sum_{a,b} \int dx_a dx_b f_{a/p}(x_a) f_{b/p}(x_b) \hat{\sigma}(ab \to c\bar{c}[n] + W/Z + X), \tag{2}$$

where $H = J/\psi$, $\psi(2S)$, and χ_{cJ}, with $J = 0$, 1, 2, and n runs over all Fock states specified above. $\hat{\sigma}(ab \to c\bar{c}[n] + W/Z + X)$ are the partonic cross sections, evaluated as perturbative expansions in α_s; $f_{a/p}(x)$ is the parton density function (PDF) of parton a in the proton; a, b include the up, down, strange (anti)quarks, and the gluon; $\mathrm{Br}(H \to J/\psi)$ are the decay branching fractions, including

$\mathrm{Br}(J/\psi \to J/\psi) = 1$ for ease of notation. In the W case, where $W^{\pm}$ is summed over, only $n = {}^3S_1^{[8]}$ contributes at leading order (LO) in α_s.

Partial results may be found in the literature. The LO results have already been obtained two decades ago [4]. At NLO, the ${}^1S_0^{[8]}$, ${}^3S_1^{[8]}$, and ${}^3P_J^{[8]}$ channels have been considered in the W case [5], and the ${}^3S_1^{[1]}$ [6,7] and ${}^3S_1^{[8]}$ [6] channels in the Z case. We can reproduce these results, with noticeable differences only in Fig. 4 of Ref. [5] for the tree-level $c\bar{c}[{}^3\mathrm{P}_J^{[8]}] + W$ channel, and fill all gaps by providing the NLO results for the ${}^3P_J^{[1]}$ channels in the W case and the ${}^1\mathrm{S}_0^{[8]}$, ${}^3\mathrm{P}_J^{[8]}$, and ${}^3\mathrm{P}_J^{[1]}$ channels in the Z case. Unlike the preceding works, we have to consider virtual corrections to P-wave state production. Albeit P-wave state virtual corrections have been tackled for single inclusive production, the additional W/Z mass scale elevates the complexity of this NLO NRQCD calculation to an unprecedented level.

Let us now review the main technical aspects of our calculation, starting with the treatment of γ_5, which appears in the W and Z axial-vector couplings and in the spin projection onto the ${}^1\mathrm{S}_0^{[8]}$ state. Adopting the standard scheme [8–11], we use the axial-vector coupling $\gamma_\mu\gamma_5$ in its antisymmetric form $\frac{1}{2}(\gamma_\mu\gamma_5 - \gamma_5\gamma_\mu)$, directly replace γ_5 by $(i/4!)\epsilon_{\mu\nu\rho\sigma}\gamma^\mu\gamma^\nu\gamma^\rho\gamma^\sigma$, employ the relation

$$\epsilon_{\mu_1\mu_2\mu_3\mu_4}\epsilon_{\nu_1\nu_2\nu_3\nu_4} = -\det(g_{\mu_i\nu_j}), \tag{3}$$

and apply the finite axial-vector coupling renormalization (see, e.g., Ref. [11]). We explicitly verify that the final results are then independent on whether we choose a D- or four-dimensional metric g in Eq. (3).

We generate, treat, and square the amplitudes using FeynArts [12] and custom FORM [13] and Mathematica codes. We reduce the virtual loop integrals to a common set of master integrals using two methods. In the first one, we directly apply integration-by-parts relations generated with AIR [14], while in the second one, we first invoke a custom Passarino-Veltman-type [15] tensor reduction, generalized for the case of arbitrary propagator powers and linearly dependent propagator momenta. We analytically check the agreement of both methods. As for the master integrals, we implement our own analytic expressions in combination with QCDLoop [16], checking everything against OneLOop [17]. We analytically simplify the resulting expressions and translate them into FORTRAN routines ready for numerical integration by our custom parallelized version of VEGAS [18]. We analytically check the ultraviolet and infrared finiteness of our results and numerically compare our real corrections, after imposing infrared cutoffs, against HELACOnia [19] output.

We organize the phase space integrations using the dipole subtraction procedure outlined in Ref. [20], changing only the momentum mapping of dipole term $V_{3,j}$ [into MapPW6 (p_j,p_2)] to cope with the presence of the massive non-QCD particle in the final state. We numerically check that all dipoles reproduce the real corrections in their respective limits and perform the check on the integrated dipoles outlined in Sec. 4. 3 of Ref. [21]. As a further check, we also implement the phase space slicing procedure along Sec. 3 of Ref. [21] to find numerical agreement. We recover the notion [21] that dipole subtraction significantly outperforms phase space slicing as for precision and speed.

We renormalize the charm quark mass in the on-shell scheme to be $m_c = 1.5$ GeV and take the charmonia to have mass $2m_c$ for definiteness. We express all electroweak couplings in terms of Fermi's constant G_F and the on-shell W and Z boson masses M_W and M_Z. We adopt from Ref. [22] the values $G_F = 1.1664 \times 10^{-5}$ GeV^{-2}, $M_W = 80.379$ GeV, $M_Z = 91.188$ GeV, $|V_{\mathrm{ud}}| = 0.9737$, $|V_{\mathrm{us}}| = 0.2245$, and all relevant branching fractions. At LO (NLO), we use the CTEQ6L1 (CTEQ6M) proton PDFs [23] with asymptotic scale parameter $\Lambda^{(4)}_{\mathrm{QCD}} = 215$ MeV (326 MeV) for $n_f = 4$ quark flavors, to be used in the one-loop (two-loop) formula for $\alpha_s^{(n_f)}(\mu_r)$, with renormalization scale μ_r.

Besides μ_r, two more unphysical scales appear, namely, the factorization scales of QCD and NRQCD, μ_f and μ_Λ. For definiteness, we put $\mu_\Lambda = m_c$ as default value and unify $\mu = \mu_r = \mu_f$, for which plausible default choices include $\mu_0 = m_{T,J/\psi}$ [5,6], $\mu_0 = \sqrt{m_{T,J/\psi} m_{T,W/Z}}$ [4], and $\mu_0 = M_{W/Z}$ [7], where $m_T = \sqrt{m^2 + p_T^2}$ is the transverse mass of a particle with mass m and transverse momentum p_T. In Fig. 1, we investigate, for each choice of μ_0, the dependencies on μ/μ_0 of the LO and NLO cross sections in Eq. (2) for ATLAS kinematics [24,25] selecting the Fock states n that already contribute at LO. We observe that the reduction in μ dependence when going from LO to NLO is least favorable for $\mu_0 = m_{T,J/\psi}$, which ignores the influence of M_W and M_Z on the scale setting. On the other hand, in the case of the important color singlet channel $pp \to c\bar{c}[{}^3S_1^{[1]}] + Z + X$, the difference between the LO and NLO cross sections is particularly small for the democratic choice $\mu_0 = \sqrt{m_{T,J/\psi} m_{T,W/Z}}$, which we thus adopt henceforth.

The experimental data as presented in Refs. [24–26] are not directly suitable for comparisons with our theoretical predictions. First, they include contributions from double parton scattering (DPS), where two partons out of the same proton participate in the hard collision, while our predictions only include single parton scattering (SPS). Fortunately, in Refs. [24–26], the DPS contributions have been estimated for each bin, using as input the universal DPS effective area $\sigma_{\mathrm{eff}} = 15^{+5.8}_{-4.2}$ mb measured in Ref. [27], so that we can conveniently subtract them out from the measured cross sections. Second, the $J/\psi + W/Z + X$

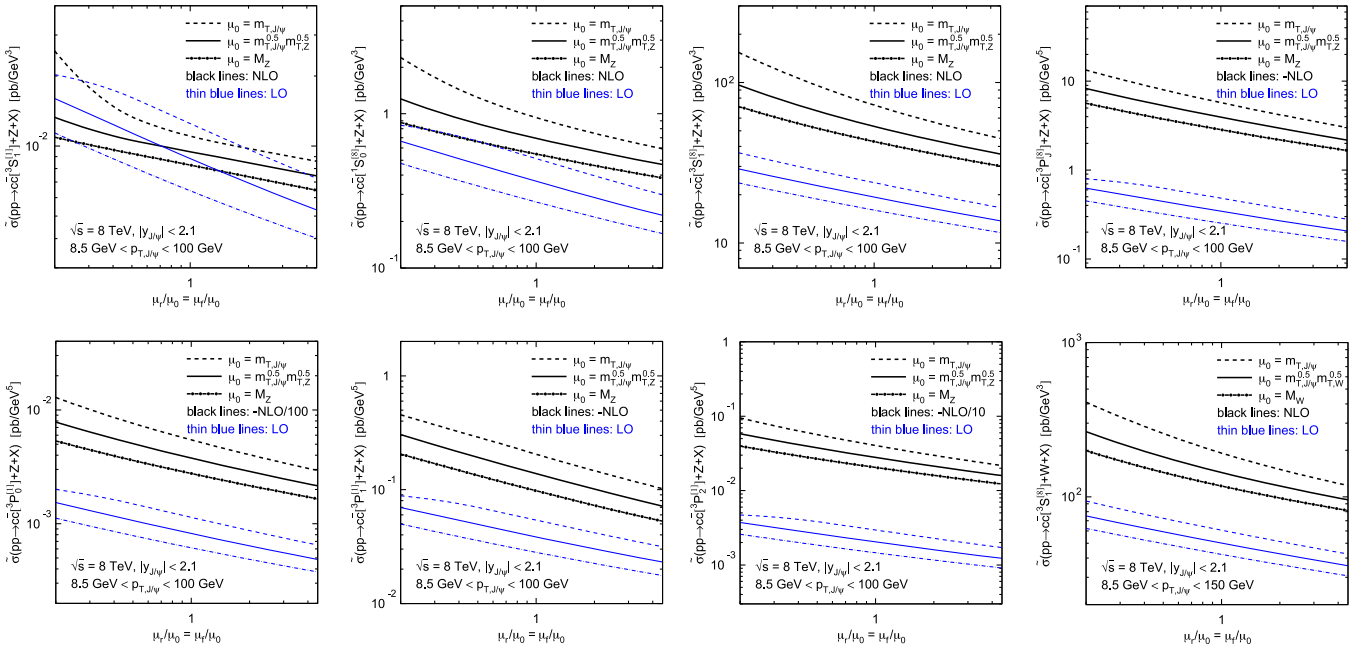

FIG. 1. Dependences on μ/μ_0, for $\mu_0 = m_{T,J/\psi}$, $\sqrt{m_{T,J/\psi} m_{T,W/Z}}$, $M_{W/Z}$, of the LO and NLO cross sections in Eq. (2) for ATLAS kinematics [24,25] selecting the Fock states n that already contribute at LO.

cross section data are in Refs. [24–26] normalized to the total cross sections, $\sigma_W = \sigma(pp \to W + X)$ and $\sigma_Z = \sigma(pp \to Z + X)$, respectively. To undo the normalization, in the W case, we rely on the ATLAS [28] and CMS [29] measurements of $\sigma_W \times \mathrm{Br}(W \to l\nu)$ at $\sqrt{s} = 7$ and 8 TeV, respectively. In the Z case, we resort to the CMS measurement of $\sigma_Z \times \mathrm{Br}(Z \to l^+ l^-)$ at $\sqrt{s} = 8$ TeV [29], which is, however, bound to include a non-negligible number of γ^* background events due to the relatively large l^+l^- invariant mass acceptance cut of 60 GeV $< m_{l^+l^-} <$ 120 GeV. This background has been estimated to be 3% using Monte Carlo simulations in Ref. [29]. On the other hand, thanks to the much tighter $m_{l^+l^-}$ cut, of just ± 10 GeV around the Z peak, the measurement of Ref. [24] should hardly be contaminated by γ^* events. To correct for this mismatch, we subtract 3% from the result for $\sigma_Z \times \mathrm{Br}(Z \to l^+ l^-)$ in Ref. [29]. To summarize, we have $\sigma_W = (98.71 \pm 2.34)$ nb at $\sqrt{s} = 7$ TeV, and $\sigma_W = (112.43 \pm 3.81)$ nb and $\sigma_Z = (33.14 \pm 1.19)$ nb at $\sqrt{s} = 8$ TeV.

We employ four popular NLO LDME sets, in which the CS LDMEs have been evaluated using potential models or extracted from measured leptonic decay rates and the CO LDMEs have been fitted to experimental data of single inclusive production, with different data selections and fit strategies. Set 1 is a combination of (i) the J/ψ LDMEs obtained by a global fit to prompt production data, with $p_T > 1$ GeV for photoproduction and two-photon scattering and $p_T > 3$ GeV for hadroproduction, after subtracting the estimated feed-down contributions [30]; (ii) the $\psi(2S)$ LDMEs recently determined from a global fit to data of unpolarized hadroproduction with $p_T > 1$ GeV [31]; and (iii) the χ_{cJ} LDMEs determined in Ref. [32] from a fit to Tevatron data with $p_T > 4$ GeV of the χ_{c2} to χ_{c1} cross section ratio. Set 2 [33] has been fitted to prompt production data with $p_T > 7$ GeV from the Tevatron and the LHC. Set 3 [34] has been fitted to prompt production data, with $p_T > 10$ GeV for J/ψ mesons and $p_T > 11$ GeV for χ_{cJ} and $\psi(2S)$ mesons, from the Tevatron and the LHC, combining fixed-order results with fragmentation contributions computed in the leading-power factorization formalism and thus resumming logarithms of $p_T^2/(2m_c)^2$. Set 4 [35] has been determined by a joint fit to LHC data of prompt J/ψ, $\psi(2S)$, $\Upsilon(2S)$, and $\Upsilon(3S)$ production, imposing $p_T > 9$ GeV for charmonium and $p_T > 28.5$ GeV for bottomonium, subtracting estimated χ_{cJ} feed-down contributions, and implementing constraints from a potential NRQCD analysis of the LDMEs. Since Ref. [35] does not provide χ_{cJ} LDMEs, we set them to zero keeping the omission of the χ_{cJ} feed-down contributions in mind as an unaccounted source of systematic uncertainty.

To enable interested readers to perform comparisons with alternative LDME sets, we list in Table I the LO and NLO default cross sections $d\tilde{\sigma}(pp \to c\bar{c}[n] + W/Z + X)/dp_{T,J/\psi} \times \mathrm{Br}(J/\psi \to \mu^+\mu^-)$ of Eq. (2) assuming the ATLAS kinematic setup at $\sqrt{s} = 8$ TeV [24,25] including the binning in $p_{T,J/\psi}$. Figure 1 and Table I also usefully portray the anatomy of the NLO corrections in the various n channels for sign and magnitude. The NLO NRQCD predictions are likely to be more reliable in the Z case than in the W case, where we expect large next-to-next-to-leading-order contributions due to the delayed unfolding of

TABLE I. LO and NLO cross sections $d\tilde{\sigma}(pp \to c\bar{c}[n] + W/Z + X)/dp_{T,J/\psi} \times \mathrm{Br}(J/\psi \to \mu^+\mu^-)$ of Eq. (2) for all contributing Fock states n in fb/GeV^4 (fb/GeV^6) for S (P) wave states, assuming the ATLAS kinematic conditions at $\sqrt{s} = 8$ TeV [24,25] including the binning in $p_{T,J/\psi}$. The common shorthand notation $d\tilde{\sigma}(pp \to c\bar{c}[^3\mathrm{P}_J^{[8]}] + W/Z + X)$ implies $\sum_{J=0}^{2}(2J+1)d\tilde{\sigma}(pp \to c\bar{c}[^3\mathrm{P}_J^{[8]}] + W/Z + X)$. The integration accuracy is around 1%.

	$pp \to c\bar{c}[n] + Z + X$					$pp \to c\bar{c}[n] + W + X$					
$p_{T,J/\psi}$ [GeV]	8.5–10	10–14	14–18	18–30	30–100	8.5–10	10–14	14–18	18–30	30–60	60–150
$n = {}^3S_1^{[1]}$, LO	0.0862	0.0488	0.0228	0.00731	0.000334	0	0	0	0	0	0
$n = {}^3S_1^{[1]}$, NLO	0.0806	0.0489	0.0251	0.00906	0.000558	0	0	0	0	0	0
$n = {}^1S_0^{[8]}$, LO	3.07	1.91	0.985	0.349	0.0202	0	0	0	0	0	0
$n = {}^1S_0^{[8]}$, NLO	5.88	3.56	1.80	0.648	0.0443	8.49	4.59	2.11	0.722	0.111	0.00604
$n = {}^3S_1^{[8]}$, LO	127	83.7	48.6	21.7	2.48	338	220	126	55.0	11.8	0.919
$n = {}^3S_1^{[8]}$, NLO	365	236	134	58.6	6.62	1000	637	361	155	33.2	2.89
$n = {}^3P_J^{[8]}$, LO	2.86	1.77	0.923	0.335	0.0208	0	0	0	0	0	0
$n = {}^3P_J^{[8]}$, NLO	−23.8	−16.2	−9.72	−4.59	−0.564	−72.0	−47.9	−28.3	−12.6	−2.81	−0.221
$n = {}^3P_0^{[1]}$, LO	0.00472	0.00339	0.00220	0.00107	0.0000942	0	0	0	0	0	0
$n = {}^3P_0^{[1]}$, NLO	−2.45	−1.63	−0.948	−0.423	−0.0477	−6.46	−4.31	−2.49	−1.09	−0.230	−0.0172
$n = {}^3P_1^{[1]}$, LO	0.323	0.206	0.106	0.0363	0.00174	0	0	0	0	0	0
$n = {}^3P_1^{[1]}$, NLO	−0.751	−0.526	−0.340	−0.171	−0.0239	−2.46	−1.75	−1.09	−0.532	−0.127	−0.0105
$n = {}^3P_2^{[1]}$, LO	0.0290	0.0117	0.00387	0.00102	0.0000531	0	0	0	0	0	0
$n = {}^3P_2^{[1]}$, NLO	−1.79	−1.19	−0.699	−0.317	−0.0371	−4.87	−3.22	−1.86	−0.823	−0.178	−0.0138

the n structure, with only $n = {}^3S_1^{[8]}$ being present at LO and $n = {}^3S_1^{[1]}$ not even at NLO.

In Fig. 2, we compare the ATLAS data [24–26], modified as explained above, to our NLO predictions for $d\sigma(pp \to J/\psi + W/Z + X)/dp_{T,J/\psi} \times \mathrm{Br}(J/\psi \to \mu^+\mu^-)$ with the same binning in $p_{T,J/\psi}$. The three rows in Fig. 2 correspond to $J/\psi + Z$ production at $\sqrt{s} = 8$ TeV [24] and $J/\psi + W$ production at 8 [25] and 7 TeV [26], the four columns to LDME sets 1–4. In each frame, we break down the total result into the contributions from the individual channels n of direct production and the combined feed-down contribution, and indicate theoretical uncertainties in the CSM and NRQCD results. The theoretical uncertainties are evaluated by adding in quadrature the errors from the following three sources: (i) variation of μ by a factor of 4 up and down relative to $\mu_0 = \sqrt{m_{T,J/\psi} m_{T,W/Z}}$; (ii) variation of μ_Λ by a factor of 2 up and down relative to m_c; (iii) quadratic combination of the individual LDME errors quoted in Refs. [30–35], making full use of the covariance matrices available from Refs. [30,31,34,35]. The large μ variation is to at least partially account for the fact that also $\mu_0 = M_{W/Z}$ is a plausible reference scale.

The default LO predictions, omitted in Fig. 2 for clarity, may be readily retrieved from Table I. The K factors at the bin level range between 0.9 and 1.7 in the CSM and between 1.7 and 2.9 (1.8 and 4.8) in full NRQCD for the Z (W) case, underpinning the above expectation regarding the speed of convergence of the perturbative expansions in both cases. Measuring the default NLO corrections in terms of the LO standard deviations, we find the ranges −0.10–0.91 in the CSM, and 1.3–3.2 (1.5–5.0) in full NRQCD for the Z (W) case. The LO and NLO error bands always overlap at least partially, except for LDME set 1 [30–32], with gaps small against the error bands themselves on logarithmic scale. This suggests that the perturbative expansions are well behaved.

We are now in a position to assess LDME sets 1–4 with regard to their ability to usefully describe the ATLAS data [24–26] at NLO in NRQCD. We immediately observe that LDME sets 2 [33] and 3 [34] lead to negative direct $J/\psi + W/Z$ production cross sections, which is physically unacceptable. They are only rescued into the positive by the feed-down contributions. Next, we observe that LDME sets 1–3 (plus the ones of Refs. [36–38], for which we refrain from showing results for lack of space) lead to predictions that throughout undershoot the data by about 1 order of magnitude. To attribute such a sizable gap to underestimated DPS contributions would require the cross sections to be overwhelmingly dominated by DPS, in contrast to the J/ψ–W/Z azimuthal-angle analyses of Refs. [24–26], which all support SPS dominance. This renders LDME

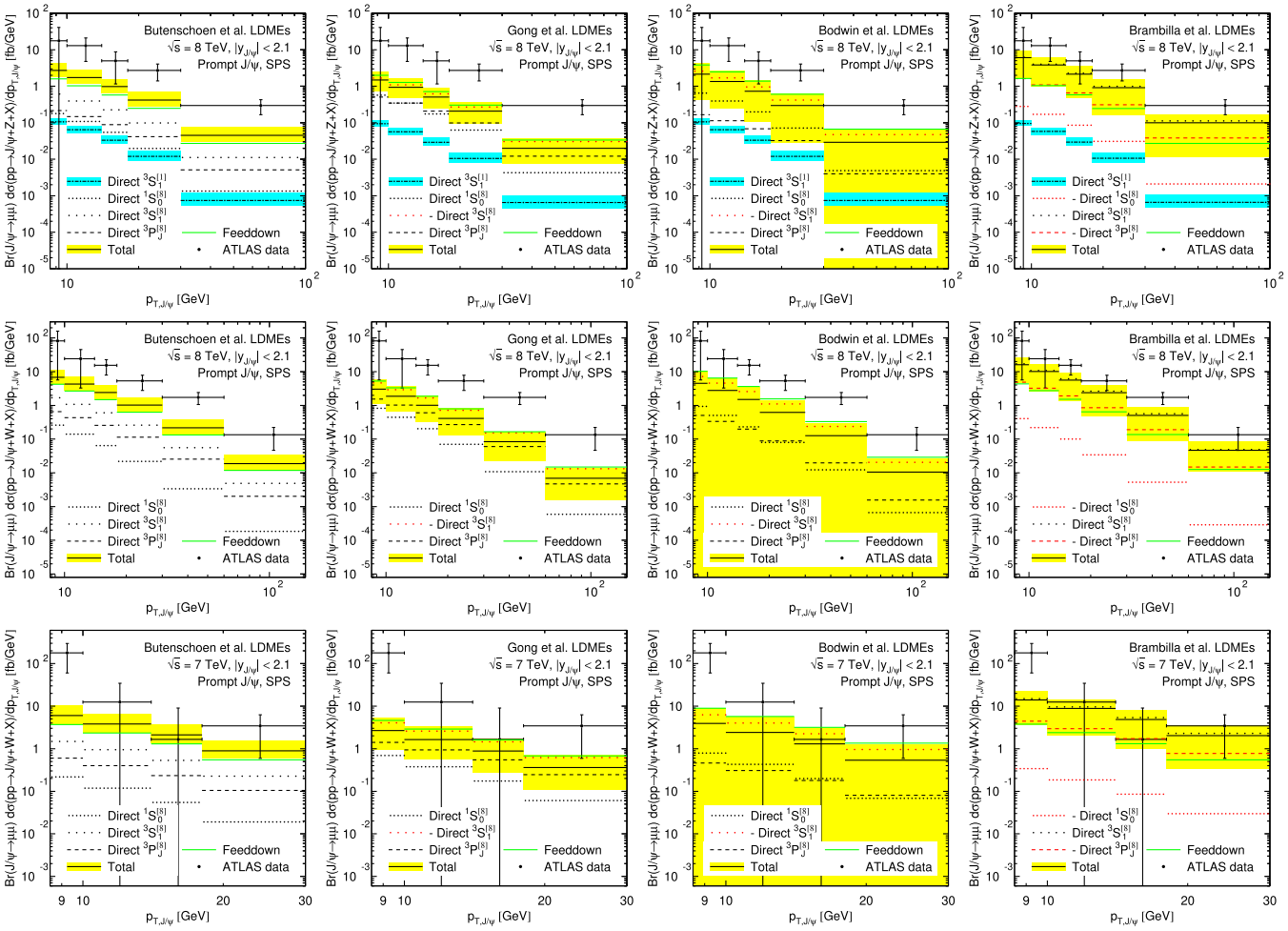

FIG. 2. Comparison of the ATLAS data from Refs. [24–26] (rows), adjusted as described in the text, to our NLO predictions for $d\sigma(pp \to J/\psi + W/Z + X)/dp_{T,J/\psi} \times \mathrm{Br}(J/\psi \to \mu^+\mu^-)$ in fb/GeV evaluated successively with LDME sets 1–4 (columns). The theoretical-uncertainty bands are evaluated as described in the text.

set 1 unfavorable, albeit not invalid. On the other hand, LDME set 4 [35] leads to an underestimation of the data by only a factor of about 3, with experimental and theoretical uncertainties typically touching or overlapping. We note in passing that this and the other LDME set determined in Ref. [35] have, however, their own problems in applications beyond the scope of this Letter, including negative NLO predictions for the LHCb measurement of prompt η_c production [39] and overshoot of HERA photoproduction data by 1 order of magnitude. Furthermore, they involve a delicate fine-tuning of negative ${}^3P_J^{[8]}$ and positive ${}^3S_1^{[8]}$ J/ψ hadroproduction channels canceling to around 90%.

To summarize, we have presented the first complete NLO NRQCD predictions of prompt-J/ψ plus W/Z associated hadroproduction, tackling P-wave loop contributions with an additional large mass scale. Requiring consistency with ATLAS data [24–26] provides valuable new information on the interplay of the J/ψ, χ_{cJ}, and $\psi(2S)$ LDMEs, orthogonal to the one encoded in one-particle-inclusive charmonium production data previously fitted to [30–38], which has allowed us to critically assess the resulting LDME sets. While none of the existing LDME sets [30–38] fully agrees with the world data of prompt J/ψ yield and polarization when $J/\psi + W/Z$ hadroproduction is included, Table I will help LDME fitters to find out how far NRQCD factorization holds at NLO. The decent description [35] of the ATLAS measurement of prompt-J/ψ plus W production [25,26] provides strong evidence for the color octet mechanism and, once again, exposes the deficiency of the CSM to describe charmonium production. Our analysis thus marks an important milestone on the path of scrutinizing NRQCD factorization.

This work was supported in part by BMBF Grant No. 05H18GUCC1 and DFG Grant No. KN 365/12-1.

[1] W. E. Caswell and G. P. Lepage, Effective lagrangians for bound state problems in QED, QCD, and other field theories, Phys. Lett. **167B**, 437 (1986).

[2] G. T. Bodwin, E. Braaten, and G. P. Lepage, Rigorous QCD analysis of inclusive annihilation and production of heavy quarkonium, Phys. Rev. D **51**, 1125 (1995); Erratum, Phys. Rev. D **55**, 5853 (1997).

[3] G. P. Lepage, L. Magnea, C. Nakhleh, U. Magnea, and K. Hornbostel, Improved nonrelativistic QCD for heavy-quark physics, Phys. Rev. D **46**, 4052 (1992).

[4] B. A. Kniehl, C. P. Palisoc, and L. Zwirner, Associated production of heavy quarkonia and electroweak bosons at present and future colliders, Phys. Rev. D **66**, 114002 (2002).

[5] G. Li, M. Song, R.-Y. Zhang, and W.-G. Ma, QCD corrections to J/ψ production in association with a W boson at the LHC, Phys. Rev. D **83**, 014001 (2011).

[6] M. Song, W.-G. Ma, G. Li, R.-Y. Zhang, and L. Guo, QCD corrections to J/ψ plus Z^0-boson production at the LHC, J. High Energy Phys. 02 (2011) 071; Erratum, J. High Energy Phys. 12 (2012) 010.

[7] B. Gong, J.-P. Lansberg, C. Lorcé, and J.-X. Wang, Next-to-leading-order QCD corrections to the yields and polarisations of J/ψ and Υ directly produced in association with a Z boson at the LHC, J. High Energy Phys. 03 (2013) 115.

[8] G. 't Hooft and M. Veltman, Regularization and renormalization of gauge fields, Nucl. Phys. **B44**, 189 (1972).

[9] P. Breitenlohner and D. Maison, Dimensional renormalization and the action principle, Commun. Math. Phys. **52**, 11 (1977).

[10] S. A. Larin, The renormalization of the axial anomaly in dimensional regularization, Phys. Lett. B **303**, 113 (1993).

[11] J. C. Collins, *Renormalization: An Introduction to Renormalization, the Renormalization Group, and the Operator-Product Expansion*, (Cambridge University Press, Cambridge, 1984).

[12] T. Hahn, Generating Feynman diagrams and amplitudes with FeynArts 3, Comput. Phys. Commun. **140**, 418 (2001).

[13] J. A. M. Vermaseren, New features of FORM, arXiv:math-ph/0010025.

[14] C. Anastasiou and A. Lazopoulos, Automatic integral reduction for higher order perturbative calculations, J. High Energy Phys. 07 (2004) 046.

[15] G. Passarino and M. Veltman, One-loop corrections for e^+e^- annihilation into $\mu^+\mu^-$ in the Weinberg model, Nucl. Phys. **B160**, 151 (1979).

[16] R. K. Ellis and G. Zanderighi, Scalar one-loop integrals for QCD, J. High Energy Phys. 02 (2008) 002.

[17] A. van Hameren, OneLOop: For the evaluation of one-loop scalar functions, Comput. Phys. Commun. **182**, 2427 (2011).

[18] G. P. Lepage, A new algorithm for adaptive multidimensional integration, J. Comput. Phys. **27**, 192 (1978).

[19] H.-S. Shao, HELAC-Onia 2.0: An upgraded matrix-element and event generator for heavy quarkonium physics, Comput. Phys. Commun. **198**, 238 (2016).

[20] M. Butenschoen and B. A. Kniehl, Dipole subtraction at next-to-leading order in nonrelativistic-QCD factorization, Nucl. Phys. **B950**, 114843 (2020).

[21] M. Butenschoen and B. A. Kniehl, Dipole subtraction vs phase space slicing in NLO NRQCD heavy-quarkonium production calculations, Nucl. Phys. **B957**, 115056 (2020).

[22] P. A. Zyla *et al.* (Particle Data Group), Review of Particle Physics, Prog. Theor. Exp. Phys. **2020**, 083C01 (2020).

[23] J. Pumplin, D. R. Stump, J. Huston, H.-L. Lai, P. Nadolsky, and W.-K. Tung (CTEQ Collaboration), New Generation of Parton Distributions with Uncertainties from Global QCD Analysis, J. High Energy Phys. 07 (2002) 012.

[24] G. Aad *et al.* (ATLAS Collaboration), Observation and measurements of the production of prompt and non-prompt J/ψ mesons in association with a Z boson in pp collisions at $\sqrt{s} = 8$ TeV with the ATLAS detector, Eur. Phys. J. C **75**, 229 (2015).

[25] M. Aaboud *et al.* (ATLAS Collaboration), Measurement of J/ψ production in association with a $W^{\pm}$ boson with pp data at 8 TeV, J. High Energy Phys. 01 (2020) 095.

[26] G. Aad *et al.* (ATLAS Collaboration), Measurement of the production cross section of prompt J/ψ mesons in association with a $W^{\pm}$ boson in pp collisions at $\sqrt{s} = 7$ TeV with the ATLAS detector, J. High Energy Phys. 04 (2014) 172.

[27] G. Aad *et al.* (ATLAS Collaboration), Measurement of hard double-parton interactions in $W(\rightarrow \ell\nu) + 2$-jet events at $\sqrt{s} = 7$ TeV with the ATLAS detector, New J. Phys. **15**, 033038 (2013).

[28] M. Aaboud *et al.* (ATLAS Collaboration), Precision measurement and interpretation of inclusive W^+, W^- and Z/γ^* production cross sections with the ATLAS detector, Eur. Phys. J. C **77**, 367 (2017).

[29] S. Chatrchyan *et al.* (CMS Collaboration), Measurement of Inclusive W and Z Boson Production Cross Sections in pp Collisions at $\sqrt{s} = 8$ TeV, Phys. Rev. Lett. **112**, 191802 (2014).

[30] M. Butenschoen and B. A. Kniehl, World data of J/ψ production consolidate nonrelativistic QCD factorization at next-to-leading order, Phys. Rev. D **84**, 051501(R) (2011).

[31] M. Butenschoen and B. A. Kniehl, Global analysis of $\psi(2S)$ inclusive hadroproduction at next-to-leading order in nonrelativistic-QCD factorization, arXiv:2207.09346 [Phys. Rev. D (to be published)].

[32] Y.-Q. Ma, K. Wang, and K.-T. Chao, QCD radiative corrections to χ_{cJ} production at hadron colliders, Phys. Rev. D **83**, 111503(R) (2011).

[33] B. Gong, L.-P. Wan, J.-X. Wang, and H.-F. Zhang, Polarization for Prompt J/ψ and $\psi(2s)$ Production at the Tevatron and LHC, Phys. Rev. Lett. **110**, 042002 (2013).

[34] G. T. Bodwin, K.-T. Chao, H. S. Chung, U.-R. Kim, J. Lee, and Y.-Q. Ma, Fragmentation contributions to hadroproduction of prompt J/ψ, χ_{cJ}, and $\psi(2S)$ states, Phys. Rev. D **93**, 034041 (2016).

[35] N. Brambilla, H. S. Chung, A. Vairo, and X.-P. Wang, Production and polarization of S-wave quarkonia in potential nonrelativistic QCD, Phys. Rev. D **105**, L111503 (2022).

[36] K.-T. Chao, Y.-Q. Ma, H.-S. Shao, K. Wang, and Y.-J. Zhang, J/ψ Polarization at Hadron Colliders in Nonrelativistic QCD, Phys. Rev. Lett. **108**, 242004 (2012).

[37] H. Han, Y.-Q. Ma, C. Meng, H.-S. Shao, and K.-T. Chao, η_c Production at LHC and Implications on the Understanding of J/ψ Production, Phys. Rev. Lett. **114**, 092005 (2015).

[38] H.-F. Zhang, Z. Sun, W.-L. Sang, and R. Li, Impact of η_c Hadroproduction Data on Charmonium Production and Polarization within the Nonrelativistic QCD Framework, Phys. Rev. Lett. **114**, 092006 (2015).

[39] R. Aaij *et al.* (LHCb Collaboration), Measurement of the $\eta_c(1S)$ production cross-section in proton-proton collisions via the decay $\eta_c(1S) \to p\bar{p}$, Eur. Phys. J. C **75**, 311 (2015).